Arab J Geosci (2016) 9: 620
DOI 10.1007/s12517-016-2637-x

ORIGINAL PAPER

Geochemistry of stratabound scheelite mineralisation and associated calc-silicate rocks from Chitral, NE Hindu Kush, Pakistan

Mohammad Zahid[1,2] · **M. Q. Jan**[3] · **Charlie J. Moon**[4]

Received: 4 September 2015 / Accepted: 15 August 2016 / Published online: 30 August 2016

Abstract Tungsten mineralisation in the NE Hindu Kush terrain occurs 8 km NW of the Tirich Boundary Zone suture between Karakoram and Eastern Hindu Kush. Scheelite occurs mainly in calc-silicate rocks and subordinately in tourmalinites associated with metasediments at Miniki Gol, Chitral. The investigated area underwent two phases of deformation and was metamorphosed up to sillimanite grade, followed by the emplacement of leucogranite and hydrothermal activity. The mineral assemblages of the calc-silicate rocks, comprising clinozoisite, quartz, calcic-amphibole, plagioclase, chlorite, biotite, calcite, sphene, garnet and scheelite, clearly express a skarn type environment. The coexistence of the scheelite grains with clinozoisite and the occurrence of anomalous values of ZrO_2 and Ta_2O_5 in the scheelite grains imply a genetic link between the scheelite mineralisation and post-magmatic hydrothermal fluids. The enrichment of Zr, Hf, Be, Sn, W, Th, U, Ga, Nb, F and Y along with total REE in the scheelite-bearing calc-silicate rocks compared with the associated metasediments assigns that the rocks at Miniki Gol have undergone a pronounced hydrothermal activity. Strong positive correlations between Zr, Hf, Nb, Y, Ta, F and REE, and the mobility of REE are consistent with this consideration. Aqueous fluid inclusions in the scheelite-bearing calc-silicate rocks display very low salinity, suggesting a mixing of magmatic fluids with meteoric water. The formation of intergrown scheelite and clinozoisite indicates a high pH and CO_2-deficient fluid. The tungsten mineralization may be related to the Miniki Gol leucogranite which occurs at a distance of only 400 m.

Keywords Scheelite · Mineralisation · Calc-silicate rocks · Fluid inclusion · Geochemistry · Chitral · Hindu Kush

✉ Mohammad Zahid
mzahid56@yahoo.co.uk

[1] Department of Geology, University of Peshawar, Peshawar 25120, Pakistan

[2] Department of Earth Sciences, CIIT, Abbottabad 22060, Pakistan

[3] National Centre of Excellence in Geology, University of Peshawar 25130 & COMSTECH Secretariat, Islamabad 44000, Pakistan

[4] Camborne School of Mines, The University of Exter, Cornwall Campus, Penryn, Cornwall TR10 9EZ, UK

Introduction

Tungsten deposits can broadly be classified into granitoid-related and non-granitoid. The first type of deposits includes tungsten-bearing granitoids, greisens, hydrothermal and tungsten skarn deposits (e.g. Hosking 1982; Raith and Prochaska 1995). In contrast, non-granitoid deposits include volcanogenic or exhalative tungsten deposits that may be remobilised by subsequent metamorphism. Examples include carbonate-hosted scheelite and wolframite of the Nock Mountains, Austria (Neinavaie et al. 1989), Western Hohe Tauern, Eastern Alps (Niedermayr and Schroll 1983) and Mittersill and Bohemian Massif, Austria (Thalhammer et al. 1989; Beran et al. 1985). Scheelite in the Bohemian Massif and Eastern Alps is associated with calc-silicate rocks, pelitic metasediments, quartzite and tourmalinite of higher amphibolite facies.

The tungsten mineralisation under discussion occurs around Miniki Gol, Chitral District, northern Pakistan. Miniki Gol lies within the NE Hindu Kush Range, some 8 km NW of Tirich Boundary Zone that is considered as suture zone between the Karakorum and Eastern Hindu Kush by Zanchi et al. (2000). The mineralisation is mainly represented by scheelite that is particularly concentrated in calc-silicate

rocks and subordinate tourmalinites. The best grade tungsten mineralisation zone is confined to a 2-km wide belt in the vicinity of Miniki Gol. Potential ore-forming two-mica leucogranite (Garam Chashma pluton) is emplaced 400 m to the southeast of the mineralised zone (Figs. 1 and 2). The Garam Chashma pluton has been dated at 22 Ma (Faisal et al. 2015; Hilderband et al. 1998). Pegmatite pockets occur within the leucogranite and associated metasediments. Moreover, marble-hosted stratiform zinc-lead mineralisation of Besti Gol is located 10 km to the NNE of Miniki Gol scheelite deposits (Fig. 1).

The rocks of the investigated area belong mostly to the Arkari Formation of probable Jurassic age (Leake et al. 1989). These, dominantly metasedimentary, rocks include garnet-mica schist, graphitic schist, carbonaceous material, phyllite, micaceous quartzite, calc-silicate rocks and carbonates (Fig. 2). The garnet-mica schist locally contains patches of tourmalinites. These rocks are metamorphosed up to amphibolite facies and have undergone at least two phases of deformation related to continental collision during the Late Cretaceous and Eocene, (Leake et al. 1989; Heuberger et al. 2007; Zanchi and Gaetani 2011).

The leucogranite and tungsten mineralization do not appear to be spatially associated at least on the surface; however, a possible genetic linkage between the two cannot be ruled out (Zahid et al. 2013). Based on mineralogical and geochemical investigation of the scheelite-bearing calc-silicate rocks and tourmalinites along with barren metasediments, the current study explains the genesis of the tungsten mineralization.

Elsewhere in Pakistan, scheelite has been reported in Saindak area in Balochistan and Oghi in Hazara, NW Himalaya. In Saindak, scheelite is associated with a pyroclastic sequence, quartz porphyry dykes and tourmaline intrusive breccia pipes. Siddiqui et al. (1986, 2012) have considered it as a hypogene mineralisation associated with the Creto-Tertiary Chagai calc-alkaline magmatic belt. Scheelite in the Oghi area has been noted in granite gneiss (Asrarullah 1982) and seems to be related to the Mansehra granite which has a Rb-Sr age of 516 ± 16 Ma (Le Fort et al. 1980).

Geology of the area

The Eastern Hindu Kush terrain, hosting the tungsten mineralization in Chitral, runs from northeastern Afghanistan to north-western Pakistan (Fig. 1) and joins the Karakoram Range to the east. Two main blocks crop out in Chitral: the western part of the Karakoram block between the Tirich Mir Fault Zone and Reshun Fault, and the East Hindu Kush block northwest of the Tirich Mir Fault (Fig. 1). Lying 20 km to the east of the mineralised zone, the Tirich Boundary Zone (TBZ) separates the Karakoram block from East Hindu Kush-Wakhan (Zanchi and Gaetani 2011). The TBZ comprises amphibolites, metagabbros, peridotites, serpentinites, gneisses and quartzites, and is considered as Jurassic-Early Cretaceous in age.

The rock units between TBZ and Reshun Fault comprise metasediments (Fig. 1) and are mainly composed of highly strained phyllite and graphitic schists adjacent to Reshun Fault. Carbonate-rich lenses within these phyllites are common (Hildebrand et al. 2000). Along the Arkari valley, Leake et al. (1989) outline the Sewakht Formation north of the Cretaceous Krinji Limestone (Desio 1966). The formation comprises greenschists, limestones, dolomitic carbonates and sandstones which may correlate with the western continuation of the Devonian Owir Series. Leake et al. (1989) also introduced the term Lutkho Formation for the monotonous greenish phyllites extending between the Sewakt Formation and the Tirich Mir pluton. These rocks have been previously considered by Pudsey et al. (1985) as Lun Shales.

The rocks between the Tirich Boundary Zone and the Afghanistan border are metapelites which are commonly highly graphitic. They are interlayered with occasional quartz-rich lenses, calc-silicates and amphibolites. These lithologies are probably the southwestward continuation of the Wakhan slates, which have yielded Palaeozoic fossils (Buchroithner 1980; Gaetani and Leven 1993). In this area, the Wakhan slates pass into composite metamorphic succession reaching up to amphibolite grade, named as Arkari Formation by Leake et al. (1989). The formation includes mica schists, phyllites, marbles, quartzites and feldspathic gneisses. The Arkari Formation hosts the studied scheelite-bearing calc-silicate rocks (Fig. 2). Based on the Belemnite remains found 75 years ago near Besti, Tipper in Pascoe (1924) had suggested a Jurassic age for at least part of the protolith of the metamorphic complex.

Metamorphism and deformation history

The Eastern Hindu Kush has experienced at least two episodes of deformation along with two distinct metamorphic phases (Leake et al. 1989; Hildebrand et al. 2001). The earlier phase of metamorphism took place prior to the D2 deformation. Typical pre-D2 metapelite assemblages contain garnet, staurolite, biotite, quartz, muscovite, plagioclase, graphite, andalusite, tourmaline, apatite and monazite. Deformation phases have been recorded in the scheelite-bearing tourmalinites; at Miniki Gol, the muscovite flakes in these define S1 foliation and crenulation displays S2 foliation (Fig. 3a).

Metamorphic mineral assemblages have been studied in only two areas including the Tirich Mir Boundary Zone and the upper Lutkho valley (Hildebrand et al. 2001). In both places, this later metamorphism is characterised by the appearance of sillimanite at the expense of staurolite and partial annealing of S1 by late mica growth (Hildebrand et al.

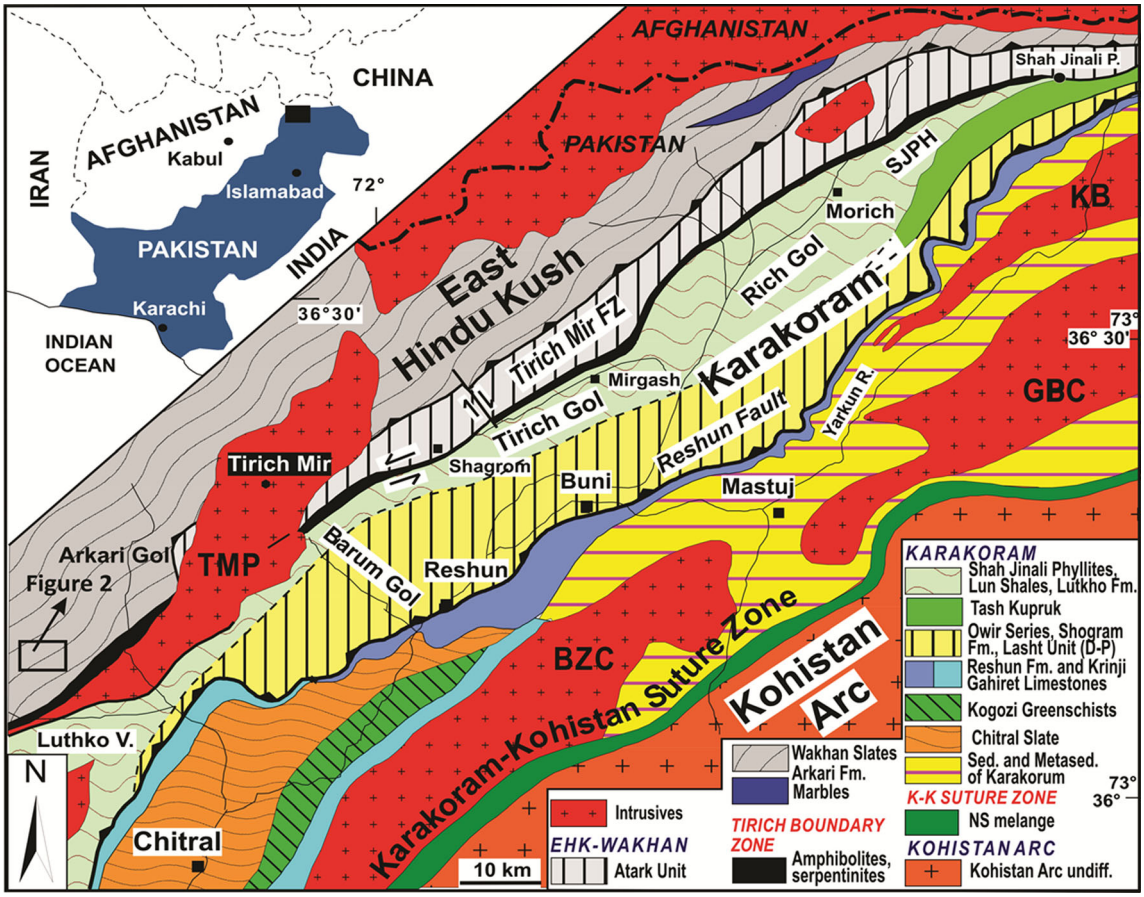

Fig. 1 Simplified geological map of the Chitral area (after Zanchi and Gaetani 2011). The box in the Arkari Gol shows the location of the investigated area at Miniki Gol

2001). Staurolite has been replaced by fibrolite and muscovite laths along the traverse from Gharam Chashma to the Tirich Mir Boundary Zone. The upper Lutkho valley is characterised by sillimanite K-feldspar schists, gneisses and migmatites.

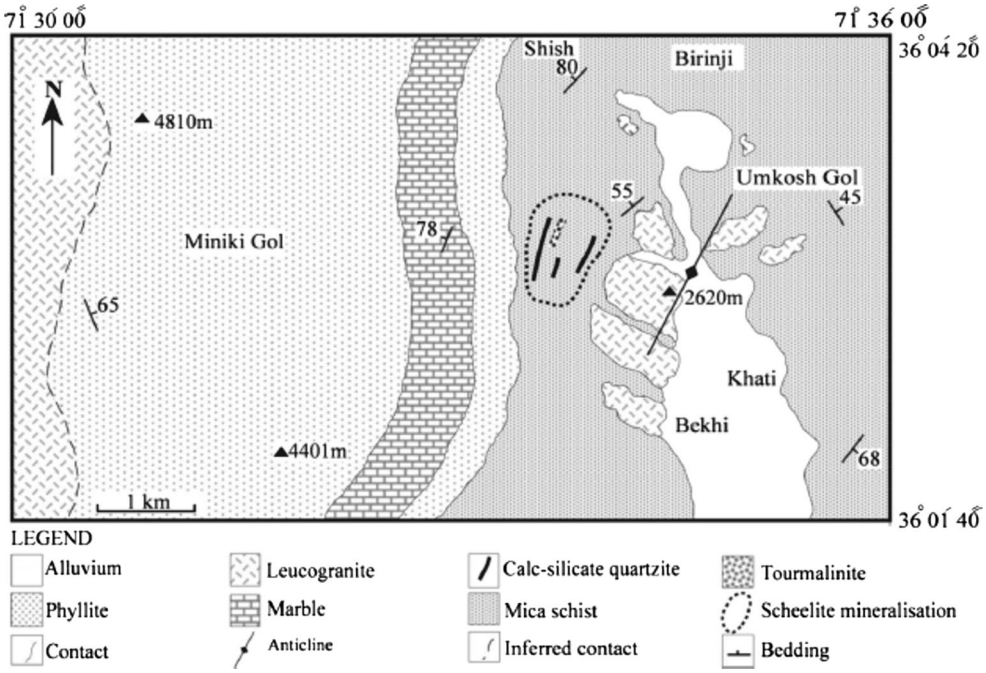

Fig. 2 Simplified geological map of the Miniki Gol and adjoining area

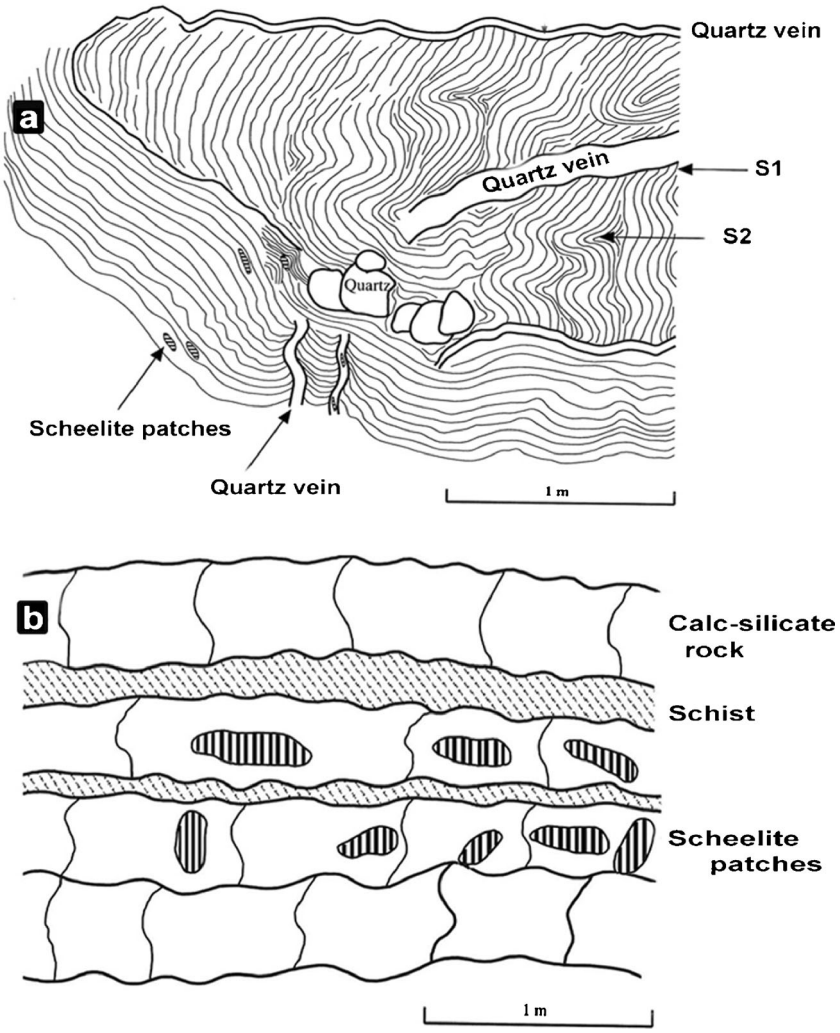

Fig. 3 **a** Sketch of tourmalinite showing overprint foliation (S1), crenulation cleavage (S2), quartz veins and scheelite patches. Note that some scheelite patches are emplaced within the quartz veins and S2 foliation. **b** sketch of schist and calc-silicate rocks containing concordant and discordant scheelite patches at Miniki Gol

The abundant intrusions of leucogranite signify crustal melting and the generation of leucogranite seems to be contemporaneous with the second deformation (D2) (Leake et al. 1989).

Tungsten mineralisation

Scheelite in the study area occurs mainly in the calc-silicate rocks and subordinately in tourmalinites. It forms discontinuous patches, stringers and conformable small veins within the calc-silicate rocks and can be considered as stratabound type (Figs. 3b and 4a). In the tourmalinites, it occurs as finely disseminated grains as well as lenses (Fig. 3a). These tourmalinites are located at three sites within 2 km strike length and comprise tourmaline (up to 80 % by volume), garnet and quartz. The occurrence of scheelite in the drag folded sections and along the axial planes of S2 suggests that it developed during the second phase of deformation when the Miniki Gol leucogranite was also intruded (Fig. 3a). Some scheelite lenses occur within the crosscutting quartz veins (Fig. 3a) indicating post-magmatic development. The study area has undergone, at least, two major deformational events (D1, D2), with associated foliations S1 and S2 (Fig. 3a).

The calc-silicate rocks are mainly composed of clinozoisite, quartz, calcic-amphibole and plagioclase. Clinozoisite grains are secondary in character and are intergrown with scheelite (Fig. 5a). Some scheelite veins also cut across the early formed main clinozoisite phase (Fig. 4b). Other ore minerals associated with scheelite include pyrite (partly altered to goethite), chalcopyrite, pyrrhotite and melnikovite (Leake et al. 1989).

The minor occurrences and showings of scheelite mineralisation extend along strike length for 7 km up to Garam Chashma. However, the best grade tungsten mineralisation zone is confined to a 2-km belt in the vicinity of Miniki Gol leucogranite

The length of the scheelite lenses reaches up to 55 cm whereas the width and thickness of these patches extends up to 14 and 12 cm, respectively (Figs. 3 and 4). The average

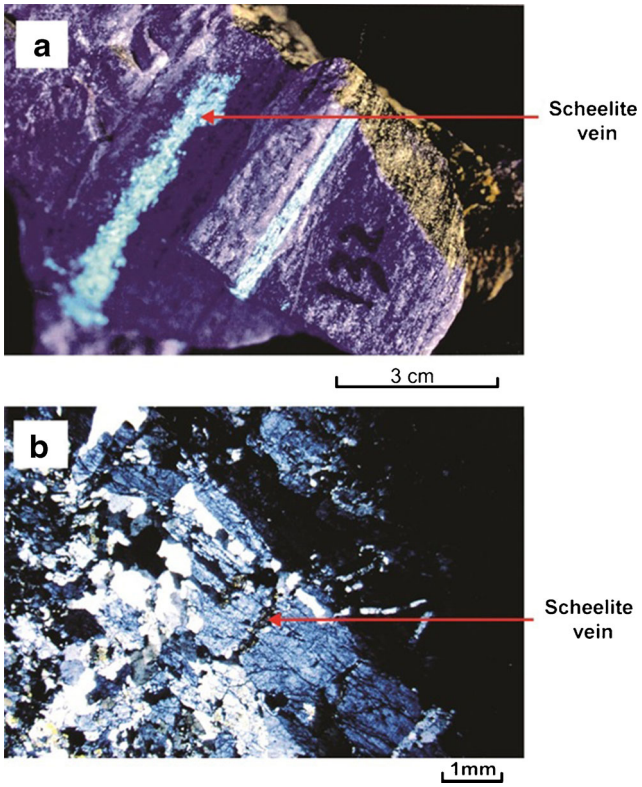

Fig. 4 **a** Florescent scheelite veins within the calc-silicate rocks along the bedding. **b** Photomicrograph showing small scheelite vein cross-cutting clinozoisite (*blue*) grains

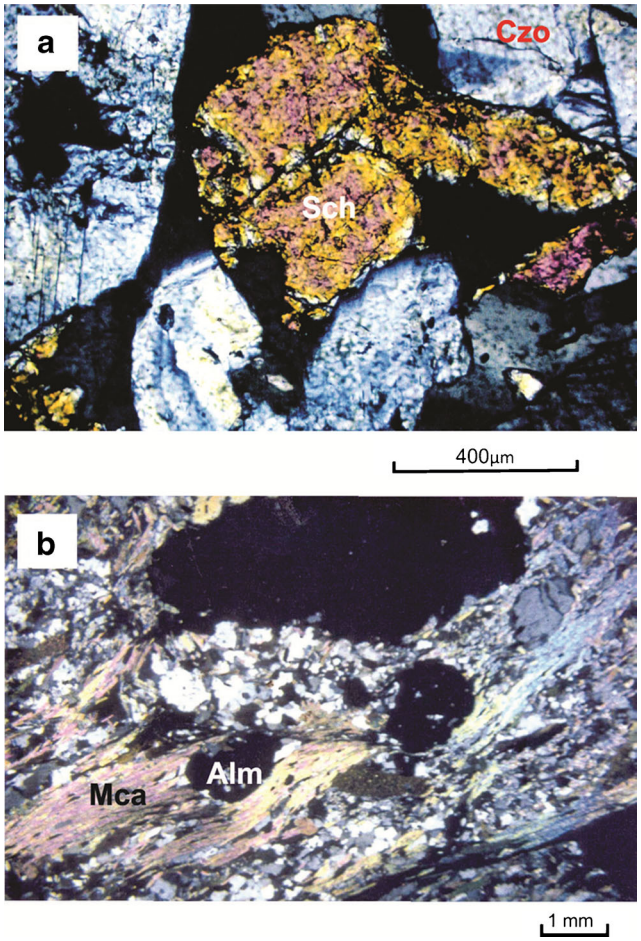

Fig. 5 Photomicrographs showing **a** scheelite grains (*Sch*) intergrown with clinozoisite (*Czo*) in calc-silicate rock, and **b** almandine (*Alm*) garnet porphyroblasts enclosed by biotite and muscovite (*Mca*) within garnet mica schist at Miniki Gol

grade of mineralisation is around 1 %, with high concentration (up to 3 %) at Miniki Gol according to our study (Table 2). The mineralisation does not seem to be economical at least on the surface because of the limited concentration of the ore even in the more promising 2-km belt near the exposed leucogranite. An exploratory drilling is required to estimate the actual ore reserve tonnage.

Sampling methods and analytical techniques

Forty three samples, representing both the scheelite-bearing calc-silicate rocks and barren metasediments, were made into polished thin sections for detailed investigation with EPMA at the University of Leicester (UK). The analyses were performed through Jeol Superprobe model JXA-8600, with an on-line computer for ZAF corrections, using wavelength dispersive system. Scheelite was analysed by a program consisting of CaO, WO_3, MoO_2, SnO_2,

FeO (total), MnO, MgO, Y_2O_3, TiO_2, ZrO_2, Nb_2O_5 and Ta_2O_5. Pure synthetic metals were used for each of W, Mo, Sn, Nb, Ta and magnetite (synthetic) for Fe. The accuracy of the ZAF correction is generally better than 2 %.

For XRF Spectrometry, 15 g powdered sample was mixed in a glass beaker with mount (10 to 20 drops) of Mowiol 88 (a solution of polyvinyl alcohol in a 1:5 mix of methanol and distilled deionised water). This mixture was then placed in a small dye and pressed into the shape of pellet. The powder pellets were run through a Philips Pw 1400 XRF spectrometer equipped with either a 3 kW rhodium anode tube or a tungsten anode tube. Each sample was analysed for Ga, Sc, Co, Ni, Cr, V, Cu, Mo, Sn, W, As, Pb, Zn, Th, Ba, Rb, Sr, Nb, Y, Zr, La, Ce, Nd, F, Cl and S. A set of international and internal standards was run with samples to monitor accuracy. The analytical results demonstrate a high degree of machine accuracy and precision (i.e., greater than 2 % at the 98 % confidence level) for all the major oxides as well as most of the minor and trace elements.

The powdered samples were also analysed for Be and Li by (ICPES). For these, 0.1 g of each sample was weighed into a labelled PTFE test tube to which 2 ml of HNO_3 (70 %) was added. All test tubes were put in a heating block at 50 °C and left overnight. Then 1 ml of $HClO_3$ (60 %) and 5 ml of HF (40 %) were added to each tube and mixed gently. This was followed by heating of the tubes in the block successively at

100 °C for 3 h, 140 °C for 3 h and 190 °C overnight. After this, 1 ml of conc. HCl was added and the tubes were heated at 50 °C. The samples were mixed thoroughly with deionised water. All tubes were decanted into 10-ml-labelled vials. The solutions were run through a Philips PV 8050 spectrometer linked to a PV 8490 source. The degree of precision and accuracy of the method was quantified by repeating 10 % of the analysed samples and 5 % of an internal standard. These estimates were later used to correct the data with the help of an "Excel Macro".

Samples from calc-silicate rocks were analysed by instrumental neutron activation analysis for REE, B, Ag, Cs, Hf, Hg, Sb, Ta, Th, U and W. The analyses were performed at the Activation Laboratories in Ontario, Canada by the procedure of Lindstrom and Anderson (1985). In this method, 0.5 to 30 g of sample, encapsulated in a polythene vial, is placed in a beam of thermalised neutrons. Samples were counted with a high purity Ge detector and loss-free counting system for the Doppler prompt gamma at 477.6 KeV. Net peak areas were adjusted for Na interference.

Fluid inclusion studies were made at Royal Holloway and Bedford New College, University of London. For the thermometric studies, doubly polished wafers were analysed using a Linkam TH 600 programmable heating-freezing stage attached to a Zeiss transmitted-light microscope. The stage has a wide range of temperature between 180 and 600 °C with the following accuracy: (1) −180 to −20 °C = ±0.1 °C, (2) −20 to +50 °C = ±0.2 °C (3) 50 to 500 °C = ±0.5 °C. The stage was calibrated using synthetic fluid inclusions in quartz crystals.

Mineralogy and petrography

Calc-silicate rocks and metasediments

The calc-silicate rocks, hosting the bulk of the scheelite mineralization at Miniki Gol, are composed of clinozoisite, quartz, calcic-amphibole, plagioclase, and small quantities of chlorite, biotite, calcite, sphene, garnet and scheelite. The clinozoisite, reaching up to 60 modal % in some samples, coexists with scheelite (Fig. 5a). The plagioclase seems to be primary and mostly changed into clinozoisite. Most calcite grains are primary; however, some are re-precipitated. Some calc-silicate rocks are banded, with darker layers containing higher proportions of amphibole, chlorite and clinozoisite. The non-banded or granular variety largely consists essentially of quartz and clinozoisite. Scheelite grains occur mostly in the non-banded variety.

The calc-silicate rocks are mineralogically quite distinct from the associated garnet-mica schist and micaceous quartzite (see Fig. 5 for comparison). The schist is mainly composed of almandine garnet, muscovite and biotite (Fig. 5b), whereas the micaceous quartzite consists of more than 90 % quartz. In contrast, the calc-silicate rocks comprise dominantly clinozoisite, quartz, calcic-amphibole and scheelite (Fig. 5a).

Other metasediments include phyllite, quartz-mica schist and metapsammite. The schist is composed of variable amounts of quartz, plagioclase, muscovite, biotite, graphite and tourmaline, with porphyroblasts of garnet and staurolite. Kyanite has been reported by Leake et al. (1989). The micaceous quartzite is composed of abundant granular quartz (>90 %); the remainder being biotite, muscovite, plagioclase and chlorite. In contrast, metapsammite contains less than 90 % quartz and additional plagioclase grains. Micaceous quartzite is abundant as compared to metapsammite. Some calc-silicate bands also cross-cut the micaceous quartzite and hence postdate the micaceous quartzite.

Scheelite

Scheelite from calc-silicate rocks consists mainly of CaO (20.28 to 20.80 wt%) and WO_3 (77.33 to 79.39 wt%); it is almost free of Mo, Y, Ti, Sn, Fe and Mn (Table 1). The noticeable feature of the analysed scheelite is the occurrence of substantial amounts of ZrO_2 (up to 0.46 wt%, average 0.28 %) and Ta_2O_5 (up to 0.35 wt%, average 0.15 %). Zr and Ta are usually associated with scheelite in pegmatite and similar values of Ta_2O_5 have also been reported in pegmatite-bearing scheelite from Thailand (Linnen and Williams-Jones 1993). The presence of significant amounts of ZrO_2 and Ta_2O_5 in scheelite is very rare (Zahid 1996; Zahid et al. 2013). Very high levels of Zr and Ta occur in scheelite from alkaline igneous rocks and from plutonic rocks relatively rich in soda (Deer et al. 1982; Tukiainen 1988). Tantalum concentration in scheelite seems to rise with increasing degree of differentiation of granitoid magmas (Boissavy-Vinau and Roger 1980). Taylor (1965) argued that Ta is concentrated in Zr-containing minerals from post-magmatic environments and that Zr^{4+} and Ta^{5+} replace W^{4+} and W^{6+}, respectively.

Geochemistry of calc-silicate rocks and micaceous quartzite

The geochemical data for the Miniki Gol scheelite-bearing calc-silicate rocks and barren micaceous quartzite are summarised in Table 2. The chemistry of the Miniki Gol calc-silicate rocks differs significantly from the post-Archean shale of Krauskopf (1967), by containing high levels of CaO (mean 9.1 wt%) and SiO_2 (mean 73.5 wt%) and low levels of Al_2O_3 (mean 11.0 wt%), FeO (mean 3.53 wt%), K2O (mean 0.3 wt%) and Na_2O (mean 0.4 wt%).

Compared with the schist from the study area, they are also enriched in CaO and Al_2O_3, and depleted in K_2O and Na_2O (Tables 2 and 3). A positive correlation exists between CaO

Table 1 Composition (wt%) of scheelite from the investigated calc-silicate rocks

Analy.	ZC70	ZC70	ZC70	ZC70	ZC70	ZC70	ZC70	ZC67	ZC67	ZC67	ZC67	ZC67	ZC67	ZC67	ZC67	ZC67	TR132	TR132	TR132	TR132	TR132	TR132	TR132
CaO	20.58	20.74	20.50	20.45	20.61	20.74	20.78	20.63	20.80	20.63	20.37	20.28	20.52	20.74	20.57	20.42	20.74	20.77	20.33	20.34	20.63	20.31	20.44	20.62
WO_3	78.25	78.18	77.60	78.33	77.96	78.32	78.78	78.01	79.39	76.88	78.15	78.31	77.63	77.94	78.28	77.56	77.67	77.50	78.75	78.18	77.33	77.97	77.62	77.77
MoO_2	00.06	00.10	00.06	00.06	00.02	00.09	00.02	00.06	00.01	00.04	00.04	00.06	00.01	00.06	00.06	00.00	00.06	00.09	00.08	00.02	00.05	00.04	00.06	00.07
SnO_2	00.02	00.02	00.00	00.02	00.02	00.02	00.01	00.02	00.05	00.02	00.02	00.02	00.02	00.02	00.02	00.02	00.02	00.02	00.02	00.02	00.02	00.02	00.02	00.02
FeO	00.03	00.00	00.02	00.01	00.04	00.00	00.02	00.02	00.01	00.02	00.01	00.02	00.02	00.01	00.02	00.00	00.04	00.02	00.04	00.02	00.02	00.03	00.02	00.02
MgO	00.00	00.00	00.02	00.00	00.01	00.00	00.00	00.00	00.01	00.00	00.00	00.00	00.00	00.00	00.02	00.00	00.00	00.00	00.00	00.00	00.00	00.01	00.00	00.00
MnO	00.02	00.02	00.03	00.02	00.02	00.02	00.01	00.02	00.02	00.02	00.01	00.03	00.08	00.02	00.01	00.02	00.02	00.01	00.01	00.03	00.02	00.02	00.01	00.01
Y_2O_3	00.06	00.04	00.06	00.06	00.06	00.06	00.06	00.06	00.06	00.06	00.06	00.04	00.06	00.06	00.06	00.06	00.06	00.06	00.06	00.06	00.06	00.06	00.06	00.06
TiO2	00.03	00.03	00.06	00.08	00.09	00.05	00.03	00.03	00.09	00.03	00.06	00.05	00.09	00.02	00.09	00.01	00.13	00.07	00.07	00.05	00.09	00.10	00.09	00.03
ZrO_2	00.24	00.30	00.10	00.33	00.41	00.35	00.28	00.37	00.46	00.39	00.24	00.18	00.39	00.26	00.06	00.28	00.35	00.15	00.39	00.31	00.18	00.23	00.15	00.28
Nb_2O_5	00.01	00.07	00.08	00.01	00.06	00.07	00.01	00.07	00.09	00.04	00.07	00.02	00.08	00.07	00.09	00.06	00.07	00.00	00.04	00.07	00.07	00.05	00.07	00.01
Ta_2O_5	00.05	00.05	00.12	00.16	00.19	00.26	00.19	00.18	00.18	00.25	00.18	00.05	00.21	00.05	00.25	00.09	00.11	00.35	00.24	00.13	00.09	00.11	00.19	00.02
Total	99.35	99.55	98.65	99.53	99.49	99.98	100.19	99.46	101.17	98.38	99.21	99.06	99.11	99.25	99.53	98.52	99.27	99.04	100.03	99.23	98.56	98.95	98.73	98.91

and Al_2O_3 in the calc-silicate rocks and it is likely that both these oxides are mainly contained in the clinozoisite (Fig. 6a). The CaO content of the calc-silicate rocks reaches up to 15.27 wt%, which is very high compared to the quartz-rich Phanerozoic greywacke (sandstone), Australia, or even quartz-poor greywacke where the maximum CaO is recorded as 5.52 wt% (see Taylor and McLennan 1985). The additional Ca might have been introduced into these rocks by hydrothermal fluids. A positive correlation also exists between Fe and Mg in the calc-silicate rocks (Fig. 6b).

The calc-silicate rocks are represented by high values of W, Sn, Zr and Hf, and low levels of B, F, Li, Ba, Rb, Cs, V, Cr and Zn (Table 2). The scheelite-bearing calc-silicate rocks are characterised by higher average concentration of Zr (455 ppm), Hf (16 ppm), Be (8.4 ppm), Th (24 ppm), U (6.1 ppm), Ga (31 ppm), Nb (14.7 ppm) and Y (35.3 ppm) as compared to the micaceous quartzite and schist (Tables 2 and 3). Tungsten levels are highly variable in these rocks and range from 0.4 ppm to 3 wt%. Gallium has a linear positive relationship with Y and Nb in the calc-silicate rocks (Fig. 6c–d). Very low concentrations of B (mean 4.9 ppm), Hg (<1 ppm), Sb (mean 0.7 ppm) and MnO (mean 0.1 wt%) and relatively low F (mean 770 ppm) are recorded in the scheelite-bearing calc-silicate rocks. This may be considered as an indication of the negligible role of exhalative activity (see also Sonnet et al. 1985; Plimer 1984; Maucher 1976). The depletion of Ba (Plimer 1987), coupled with low level of the P_2O_5 (mean 0.3 %) in the scheelite-bearing calc-silicate rocks, also rule out exhalative activity.

The Miniki Gol calc-silicate rocks are enriched in REE contents (Table 2) compared with the North American shale (Taylor and McLennan 1985). The total REE abundances in the scheelite-bearing calc-silicate rocks are relatively high as compared to the barren micaceous quartzite. Maximum REE contents (ppm) in the scheelite-bearing rocks shown in Table 2 are as follows: La (130), Ce (280), Nd (100), Sm (19), Eu (2.9), Gd (13), Tb (3.9), Yb (9) and Lu (1.39). Almost half of the scheelite-bearing calc-silicate rocks as well as the unmineralised micaceous quartzite exhibit positive Eu anomalies (Fig. 7a). The REE pattern of the calc-silicate rocks is more or less similar to that of Miniki Gol leucogranite (Fig. 7a, c). The calc-silicate rocks are represented by low chondrite-normalised (La/Lu) N ratios (<10) whereas in most of the analysed micaceous quartzite, (La / Lu) N ratios are greater than 10 (Table 2). The majority of the scheelite-bearing calc-silicate rocks (13 out of 21) are enriched in HREE. This enrichment is apparent from the LA/Yb ratio of less than 10. In comparison, the LA/Yb ratio in the micaceous quartzite is very high, reaching up to 19 (Table 2). A strong positive correlation exists among the REE and Zr, Hf, Nb, Y, Ta, together with a weak linear relationship with F (Fig. 8a–f). However, no correlation has been found between REE and ore elements such as W and Sn.

Table 2 Summary of the geochemical data of the Miniki Gol micaceous quartzite and calc-silicate rocks (major elements wt%)

	Micaceous quartzite					Calc-silicate rocks				
	Min	Max	Mean	Std[c]	N[d]	Min	Max	Mean	Std[c]	N[d]
SiO_2	63.9	94.9	74.7	11.4	10	60.3	92.2	73.5	09.3	23
TiO_2	00.2	00.8	00.4	00.2	10	00.1	01.3	00.6	00.3	23
Al_2O_3	03.0	17.7	07.5	05.4	10	03.5	17.1	11.0	04.2	23
Fe_2O_3[a]	00.4	04.9	01.5	01.8	10	00.9	07.2	03.5	01.6	23
MnO	00.0	00.1	00.0	00.0	10	00.0	00.5	00.1	00.1	23
MgO	00.2	01.5	00.5	00.5	10	00.2	01.8	00.8	00.4	23
CaO	00.0	04.0	01.7	01.6	10	03.3	15.3	09.1	04.0	23
Na_2O	00.2	04.1	01.8	01.5	10	00.0	01.6	00.4	00.4	23
K_2O	00.3	02.3	01.2	00.9	10	00.0	01.6	00.3	00.4	23
P_2O_5	00.0	00.3	00.1	00.1	10	00.0	01.2	00.3	00.3	23
Total	96.9	100.8	99.3	01.4	10	96.9	101.7	99.5	01.5	23
Trace elements (ppm)										
B	05.0	06.0	05.5	00.7	02	2.0	14.0	0.9	03.2	13
F	70	920	313	290	10	130	1430	770	325	31
Cl	40	80	53	14.9	10	30	220	86	65	31
S	00.0	80	15	31	10	00.0	550	100	158	31
As	01.3	01.4	01.4	00.1	02	00.5	03.8	01.6	00.8	20
Li	12	225	65	50	19	05.2	204	55	50	44
Be	00.5	08.5	02.4	02.0	19	00.5	51.5	04.3	09.2	44
Cs	03.0	09.0	06.0	04.2	02	01.0	11.0	03.9	03.4	16
Ba	21	1295	326	282	19	00.8	452	98	112	43
Rb	05.2	130	51.3	33.9	19	00.1	167	41.2	42.4	39
Sr	28.3	1148	280	258	19	47	420	212	87	44
Th	01.0	25.0	12.8	05.7	19	03.6	81.0	17.1	14.8	44
U	03.3	06.5	04.9	02.3	02	01.7	17.0	05.3	03.7	20
Zr	06.0	562	325	127	19	70	1567	350	242	44
Hf	11.0	16.0	13.5	03.5	02	03.0	46.0	12.4	10.2	21
Ta	02.3	02.3	02.3		01	00.7	04.0	01.5	00.9	13
Nb	01.1	18.1	09.0	04.0	19	03.4	24.6	12.5	05.5	44
Y	03.0	37.6	21.4	9.6	19	12.3	75.7	31.5	12.9	44
Sc	00.5	16.2	08.0	04.3	17	00.2	20.9	10.3	04.6	42
V	04.2	77.2	33.4	18.5	19	11.8	93	49.6	22.3	44
Cr	10.6	78	37	22.2	18	2.9	166	47	30	44
Co	00.5	13.0	04.2	03.5	18	01.8	27.9	10.6	05.1	43
Ni	02.1	34.7	11.9	10.3	16	02.8	90	28.3	20.0	43
Cu	01.2	18.3	07.7	05.5	10	00.4	49.2	11.4	11.3	39
Zn	01.4	193	30.0	44.6	18	06.7	93.3	37	22	40
Hg	<1	<1			02	<1	<1			21
Ag	<5	<5			02	<5	<5			21
Ga	03.0	20.4	08.7	04.0	19	3.8	70.5	19.9	12.9	42
Pb	02.5	206	27	45	19	02.0	48.7	20.3	10.1	44
W	00.1	21.0	02.7	05.5	14	00.4	30,550	3090	7290	39
Sn	01.0	39.6	06.4	10.16	17	01.2	452	64.2	114	43
Mo	00.1	03.2	01.7	00.9	19	00.0	05.0	01.2	01.2	36
Sb	00.3	00.9	00.6	00.4	02	00.2	02.0	00.7	00.6	14
La	39	44	41.5	3.5	02	08.4	130	43	29.4	21
Ce	83	86	84.5	02.1	02	20	280	89	59.7	21
Nd	24	30	27	4.2	02	10	100	35	20	20
Sm	05.5	05.8	05.7	00.2	02	01.6	19.0	06.9	03.8	21
Eu	01.1	01.6	01.4	00.4	02	00.6	02.9	01.6	00.6	21
Gd	04.0	05.0	04.5	00.7	02	01.0	013	05.1	02.9	21
Tb	00.7	00.7	00.7		01	00.7	04.9	01.9	01.3	15
Yb	02.3	03.0	02.7	00.5	02	02.0	09.0	04.4	02.0	21
Lu	00.4	00.5	00.4	00.0	02	00.2	01.4	00.6	00.3	21
Eu/Eu[b]	00.7	00.9				00.6	01.6			
La/Yb	13	19				03.2	15.6			
(La/Lu)N	08.6	10.8				02.5	09.7			

Be and Li were analysed by ICP-ES and B, Cs, U, Hf, Ta, Sb, Hg, Ag and REE by INAA. All other elements were analysed by XRF

cn chondrite-normalised value

[a] Total iron considered as Fe_2O_3

[b] Eu/Eu* (i.e. $EuN/[(SmN)\ (GdN)]_{1/2}$

[c] Standard deviation

[d] Number of samples

Schist

Summary of the major and trace elements chemistry of the schist from the Miniki Gol and surrounding area is given in Table 3. Comparison of the major element chemistry of the studied metasediments with the average post-Archean shale of Krauskopf (1967), shows that the Miniki Gol schistose rocks are richer in Na and poorer in Ca (Table 3). The CaO content of the calcite-rich schist reaches up to 9.15 wt%, whereas the garnet-rich schist contains up to 12.2 wt% FeO and 2.1 wt% MnO. Comparing the trace element data of the rocks with the average shale of Turekian and Wedepohl (1961), the Miniki Gol schist is significantly depleted in S and to a lesser extent, Cl, Ni, Cu and Mo (Table 3). The studied schist is enriched in F, Li and Cs and to a lesser extent, Be, W, Pb, Th, Zr, Y, Hf and Nb (Table 3). Leake et al. (1989) have also reported high level of B (minimum 201 ppm), W (mean 11 ppm) and As (up to 26 ppm) in the studied schist. The enrichment of these elements is a clear expression of metasomatic activity (see also Christensen et al. 1983; Leake et al. 1989; Van de Haar et al. 1993), in the Miniki Gol schist.

The REE contents of the Miniki Gol metasediments are significantly higher (Table 3, Fig. 7b) than the North American shale (see Taylor and McLennan 1985). The maximum Eu/Eu* ratios in the studied schist is observed as 0.9 (Table 3). The mobility of REE in metamorphic rocks is poorly understood (see Grauch 1989) and many investigators (e.g. Cullers et al. (1974) and Lottermoser (1989a)) consider that REE content is unaffected during progressive metamorphism. However, partial melting and retrogressive metamorphism do change (loss or gain) the REE content (cf. Lottermoser 1989a). The enrichment of REE abundances in the proposed metasediments relative to the North American shale might be indicative of metasomatic activity.

Microthermometry

Aqueous fluid inclusions were found in the Miniki Gol scheelite-bearing calc-silicate rocks (Fig. 9); however, no CO_2-bearing fluid inclusions were observed. The fluid inclusions in these rocks are smaller (15 to 20 μm in diameter) than those observed in the pegmatite and leucogranite of the area (Zahid 1996). These inclusions occur in quartz with well-defined grain boundaries and are intergrown with clinozoisite and scheelite crystals (Fig. 5a). The aqueous fluid inclusions have very low salinity, with the maximum value as 2 wt% NaCl equivalent. The salinity of CO_2-bearing fluid inclusions in the muscovite pegmatite at Miniki Gol ranges from 8 to 10 wt% NaCl equivalent, whereas the primary fluid inclusions in leucogranite are characterised by relatively low salinity (between 2 and 8 wt% NaCl equivalent). The homogenisation of the two phases in these inclusions in the calc-silicate rocks occurred at temperature between 160 °C and 500 °C (Fig. 10). The fluid inclusions in the pegmatite homogenised at maximum temperature 495 °C and in leucogranite at 440 °C. It is also worth mentioning that the salinity progressively decreases from pegmatite through leucogranite to scheelite-bearing calc-silicate rocks at Miniki Gol (Zahid 1996).

Discussion

The genesis of the Miniki Gol scheelite mineralisation and its protolith is difficult to assess as the study area has undergone multiple episodes of deformation and metamorphism, followed by the intrusion of leucogranite and post-magmatic hydrothermal activity. On the basis of high levels of Mn and Zn and low levels of K and Rb in the tourmaline-quartz gneiss compared with associated schist, Leake et al. (1989) have considered these tourmaline-rich rocks as siliceous chemical precipitates. These authors have ascribed a sedimentary/exhalative or diagenetic origin to the Miniki Gol scheelite mineralisation and argued that subsequent metamorphism recrystallised the tungsten as scheelite prior to the emplacement of leucogranite. The present study, however, suggests that hydrothermal activity has played a significant role in the transformation of micaceous quartzite into calc-silicate assemblages at Miniki Gol. The mineral paragenesis such as clinozoisite,

quartz, calcic-amphibole, plagioclase, chlorite, biotite, calcite, sphene and garnet, along with scheelite in the calc-silicate rocks, undoubtedly specifies a skarn type environment. The occurrence of clinozoisite (up to 60 % by volume), the coexistence of scheelite and clinozoisite grains (Fig. 5a), and the presence of the calc-silicate minerals indicate that hydrothermal solutions have converted the micaceous quartzites into calc-silicate rocks. The enrichment of Zr, Hf, Be, Sn, W, Th, U, Ga, Nb, F and Y in the scheelite-bearing calc-silicate rocks compared with micaceous quartzite is compatible with hydrothermal alteration. This metasomatic activity is more prominent in the scheelite-bearing calc-silicate rocks than in the unmineralised micaceous quartzite. The CaO level in the calc-silicate rocks is high (mean 9.1 wt%) as compared to the micaceous quartzite (mean 4 wt%). This shows that hydrothermal fluids have leached CaO from associated marble and reprecipitated in the calc-silicate rocks, altering micaceous quartzite into calc-silicate assemblages. The positive correlation among Ga, Nb and Y (Fig. 6c, d) in the scheelite-bearing calc-silicate rocks indicates similar geochemical behaviour of these elements during the hydrothermal regime. Moreover, the high concentrations of F, Li and Cs, and to a lesser extent Be, W, Sn, Pb, Th, Zr, Y, Hf and Nb in Miniki Gol schist (Table 3), compared with the average shale (Turekian and Wedepohl 1961), suggest that these elements have been introduced by metasomatic fluids.

Table 3 Geochemistry of the schist from Miniki Gol and surrounding area (major elements wt%)

	Min	Max	Mean	Std[b]	Number[c]	Krauskopf (1967) Average post-Archean shale
SiO_2	47.3	75.7	63.2	06.7	31	61.6
TiO_2	00.4	01.2	00.8	00.2	31	01
Al_2O_3	11.1	29.4	17.9	4.2	31	18.3
Fe_2O_3	03.8	12.2	07.1	02.3	31	07.4
MnO	00.0	02.1	00.2	00.4	31	00.13
MgO	01.2	04.4	02.4	00.7	31	02.7
CaO	00.6	09.2	03.0	02.0	31	04.2
Na_2O	00.9	7.1	02.5	01.6	31	01.1
K_2O	00.4	05.5	02.8	01.4	31	03.4
P_2O_5	00.1	00.3	00.2	00.1	31	00.22
Total	98.7	102.1	100.1	0.90	–	100.1
Trace elements (ppm)						Turekian and Wedepohl (1961) average shale
B	17	184	75	60.5	06	100
F	270	3210	1135	522	29	740
Cl	40	230	115	75	29	180
S	00.0	1390	130	279	29	2400
Li	27.5	469	190	110	43	66
Be	01.0	20.9	04.4	03.2	43	03
Cs	09.0	83	33	34.5	04	05
Ba	55.1	949.7	485.1	220.9	43	580
Rb	14	420	180	84	43	140
Sr	40	712	256	138	43	300
Th	04.8	31.6	20	06.2	43	12
U	01.8	06.4	04.7	02.2	04	03.7
Zr	110	658	210	103	43	160
Hf	03	08	06.3	02.2	04	02.8
Ta	02	03.1	01.9	00.6	03	0.8
Nb	6.9	31.1	18.8	04.5	43	11
Y	19.9	57.7	35.9	07.5	43	26
Sc	09.4	23.3	16.7	03.5	43	13
V	53.3	153	106	23	43	130
Cr	31.3	173	110	32.7	43	90
Co	09.6	41.3	20.2	07	43	19
Ni	08.5	74.4	37.8	18.4	43	68
Cu	01.2	74.2	21.8	13.6	41	45
Zn	50.5	256	100	37.4	43	95
Ga	11.3	39.4	24.8	05.8	43	19
Pb	06.7	60	31.2	11.6	43	20
W	00.4	08	3.2	02	36	01.8
Sn	01.3	16.5	05.03	03.55	43	06
Mo	00.1	03.4	00.8	00.9	37	02.6
Sb	02.2	02.9	02.6	00.4	03	01.5
La	17	92	65.3	34.5	04	92
Ce	42	180	128	63	04	59
Nd	14	59	43.3	21	04	24
Sm	02.9	14	09.5	05.1	04	06.4
Eu	00.8	02.8	02	01	04	01
Gd	02	11	05.5	04	06	06.4
Tb	02	02.4	02.2	00.3	02	01
Yb	01.9	06.3	04.6	02	04	02.6
Lu	00.3	01	00.7	00.3	04	00.7
Eu/Eu[a]	00.7	00.9				

Fe2O3 is regarded as total iron. Be and Li were analysed by ICP-ES and B, Cs, U, Hf, Ta, Sb and REE by INAA. All the other elements were analysed by XRF

n.a not analysed

[a] Eu/Eu (i.e. EuN/ $[(SmN)\ (GdN)]_{1/2}$

[b] Standard deviation

[c] Numbers of samples;

Hydrothermal activity has also affected the REE pattern of the Miniki Gol calc-silicate rocks. Some of the scheelite-bearing rocks, such as ZC 65 a (Fig. 7a), are rich in REE whereas some, such as ZC 70, are depleted in total REE

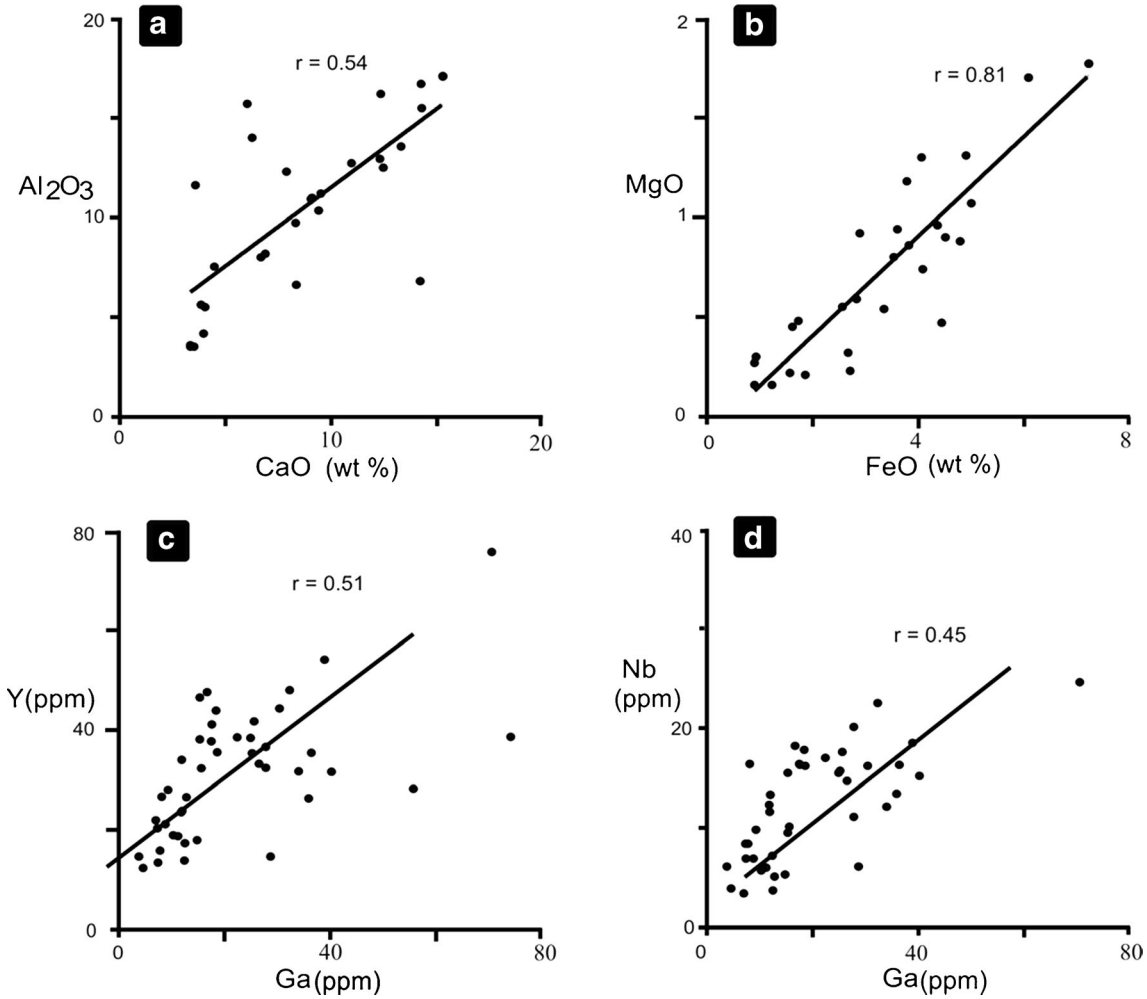

Fig. 6 **a**–**b** Relationship of oxides, CaO vs. Al_2O_3 and FeO vs. MgO, in the Miniki Gol calc-silicate rocks. **c**-**d** Correlation of Ga vs. Y and Nb in the studied calc-silicate rocks

(Fig. 7a). This enrichment and depletion of the REE in the scheelite-bearing calc-silicate rocks, enrichment of HREE over LREE and positive Eu anomalies are suggestive of a pronounced metasomatic activity in these rocks. HREE enrichment and low (La / Lu) N ratios (Table 2) demonstrate hydrothermal alteration and could be related to scheelite deposition with the decreasing temperature of the hydrothermal fluid (Lottermoser 1989b). Positive Eu anomalies have also been reported by Sonnet et al. (1985) in scheelite-bearing calc-silicate rocks of peri-granitic origin. The compatibility of the REE pattern between leucogranite and calc-silicate rocks at Miniki Gol (Fig. 7a, c) also establishes a genetic association between these two rocks. The strong correlation between the elements such as Zr, Hf, Nb, Y, Ta, F and REE (see Fig. 8) indicates an identical geochemical behaviour of these elements in the calc-silicate rocks and also suggests that REE were mobile in the aqueous fluids. The mobility of the REE appears to increases with the change from early-magmatic to late-stage hydrothermal solutions (cf. Lottermoser 1992). The fluoride and carbonate complexes can significantly facilitate the transportation of the REE along with Y in hydrothermal regime (Wood 1990). pt?>The transportation of Zr, Ti, U, Th, Y along with REE in the presence of alkali-rich-fluorine and phosphorus complexes have also been reported by Giere (1990) and Rubin et al. (1993). Moreover, both acidic and alkaline environments facilitate the transportation of H_2WO_4 and WO_4^{2-} respectively (Robb 2005). The most interesting feature of the Miniki Gol scheelite is the relatively higher levels of Zr and, to a lesser extent, Ta (up to 0.46 and 0.35 wt%, respectively). This enrichment, particularly of Ta, has been related to late-stage granitic and pegmatitic intrusions (Linnen et al. 2012; Stilling et al. 2006; Deer et al. 2013).

The occurrence of tourmalinites at three locations within 2 km strike length, the absence of Sb and Hg in the studied rocks and the lack of cinnabar-stibnite mineralisation at Miniki Gol (Zahid et al. 2013) are inconsistent with the exhalative or volcano-sedimentary origin. The lack of evidence for the presence of evaporites such as secondary halides in the study area rules out the possibility of

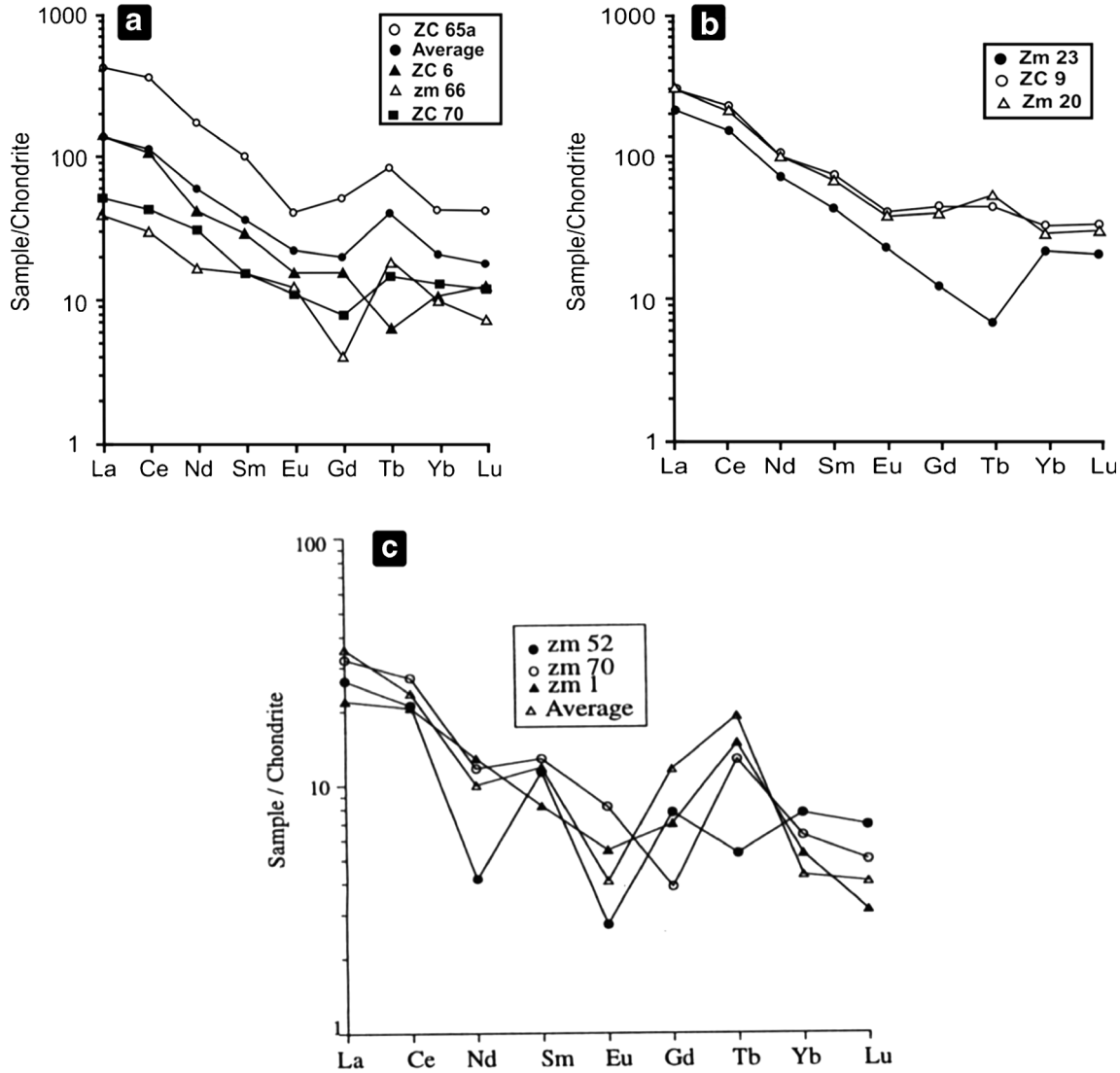

Fig. 7 Chondrite-normalised REE pattern of **a** calc-silicate rocks (zc 65a, zc 70 and zm 66 and micaceous quartzite (sample zc 6), **b** garnet mica schist, and **c** leucogranite at Miniki Gol

lacustrine environment. Boron-rich clay is also an inadequate precursor as clay minerals are not known to contain more than 2000 ppm of boron (Slack et al. 1984). This amount of boron would only be sufficient for 9 % tourmaline by volume (Plimer 1986), whereas Miniki Gol tourmalinites contain up to 80 % tourmaline by volume. Leucogranite can be considered as a potential source for the excessive boron of these tourmalinites. The mineral chemistry of tourmaline, although not conclusive, can provide some constraints on any genetic relationship between the leucogranite and tourmalinisation. The average FeO# of the tourmaline (0.6) from the Miniki Gol tourmalinites corresponds to magmatic hydrothermal (greisen-related) Sn-W deposits (cf. Zahid et al. 2013). This ratio of the tourmaline from studied tourmalinites is higher than that of the associated leucogranite, thereby reflecting an Fe-enrichment trend away from the granite as a result of late-stage evolved magmatic differentitaion (see also Benard et al. 1985; Taylor et al. 1992). Moreover, the reverse trend of chemical zoning, i.e. higher MnO in rims than cores, in the tourmaline grains from the tourmalinites at Miniki Gol corresponds to a metasomatic origin (cf. Zahid et al. 2013).

Aqueous fluid inclusions in the scheelite-bearing calc-silicate rocks are of very low salinity. A generally decreasing trend of the homogenisation temperatures from CO_2-bearing fluid inclusions to aqueous fluid inclusions within the Miniki Gol pegmatite correlates with decrease in salinity (Zahid 1996). This suggests that magmatic fluids were probably mixed with meteoric water. Such a phenomenon is a characteristic feature of many hydrothermal and greisen-related deposits, such as the tungsten deposits of Xihuashan, China (Giuliani et al. 1988) and Cligga Head, SW England (Spooner 1981). The occurrence of

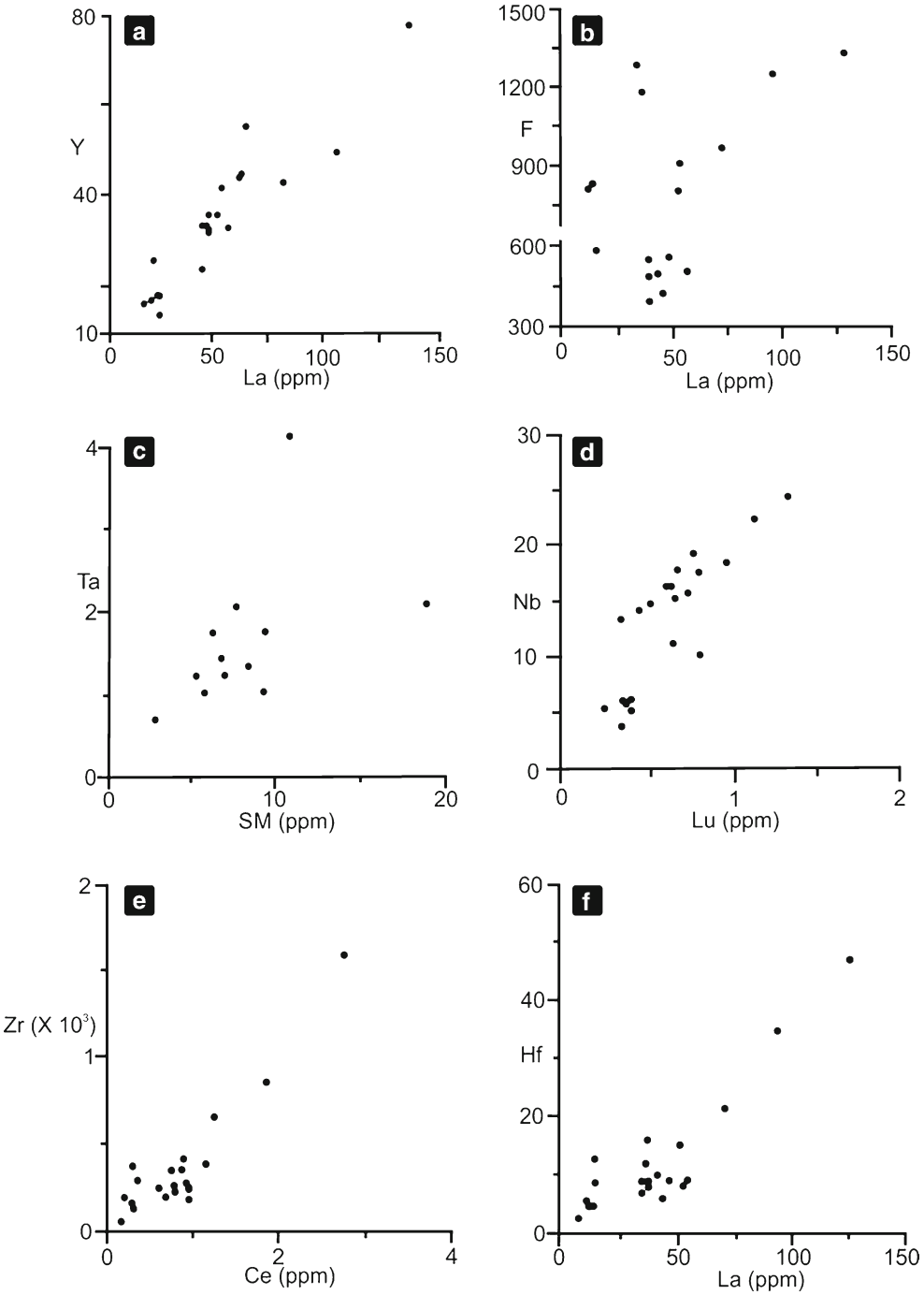

Fig. 8 Correlations of REE in calc-silicate rocks with other trace elements (ppm): **a** Yttrium, **b** Fluorine, **c** Tantalum, **d** Niobium, **e** Zirconium and **f** Hafnium. Identical relationship holds for other REE with the corresponding elements

calcite in the Miniki Gol scheelite-bearing rocks demonstrates that some CO_2 was possibly present at the early stage of the hydrothermal fluids. Tungsten was introduced into the site of deposition (calc-silicate rocks) probably during the last phase of the hydrothermal activity, when pH was relatively high. As pointed out by Absar (1991), clinozoisite usually forms from high pH and CO_2-deficient fluid whereas calcite precipitates from CO_2-rich fluids. The continuous separation and consumption of CO_2 by calcite from the hydrothermal fluid may have increased the pH of the fluid and facilitated the deposition of clinozoisite together with scheelite from the CO_2-deficient fluid. The scarcity of the CO_2-bearing fluid inclusions in the scheelite-bearing calc-silicate rocks and the association of clinozoisite with the scheelite imply that the fluid phase at the time of growth of these minerals was predominantly aqueous. This is consistent with the laboratory experiments of Keppler and Wyllie (1991) that solubility of W is very high in the presence of water as the sole volatile.

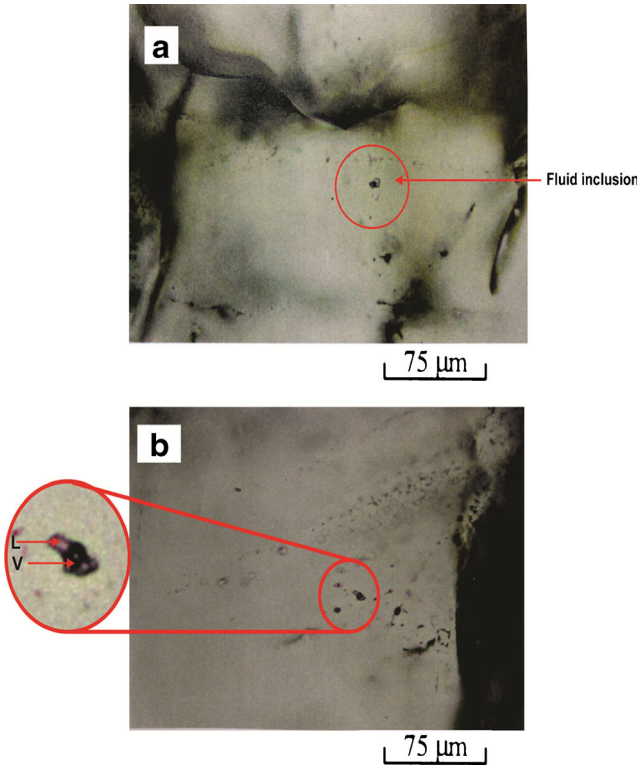

Fig. 9 Aqueous fluid inclusions in the scheelite-bearing calc-silicate rocks at Miniki Gol. **a** Fluid inclusions in the granular quartz intergrown with scheelite. **b** Aqueous fluid inclusions along with trail of mono-phase fluid inclusions in the quartz grain

Conclusions

The main conclusions derived from this study are as follows:

1. Hydrothermal fluids played a key role in the transformation of micaceous quartzite into scheelite-bearing calc-silicate mineralogy.
2. The association of clinozoisite, calcic-amphibole, plagioclase, chlorite, biotite, calcite, sphene and garnet indicates skarn style mineral assemblages.
3. The enrichment of Zr, Hf, Be, Sn, W, Th, U, Ga, Nb, F and Y, along with total REE in the scheelite-bearing calc-silicate rocks and metasediments, suggests a significant metasomatic activity at Miniki Gol.
4. It is concluded that the intergrown scheelite and clinozoisite were formed from CO_2-deficient and high-pH hydrothermal fluids.

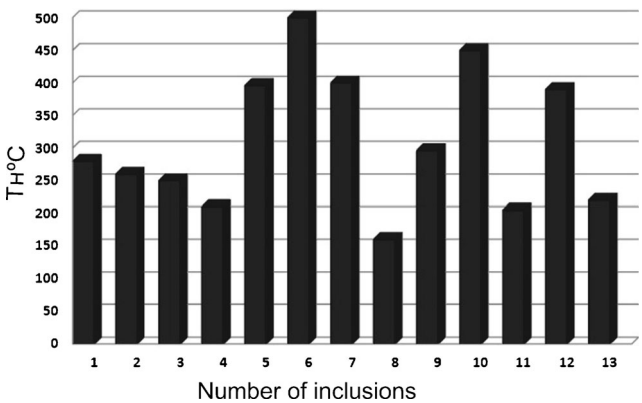

Fig. 10 Total homogenisation temperature (T_H) of Miniki Gol scheelite-bearing calc-silicate rocks

Acknowledgments The Association of the Commonwealth Universities in UK financed this study. Mr. Rob Kelly helped in preparing samples and Mr. Nick Marsh facilitated the performance of analytical work at the Department of Geology, University of Leicester, UK. Dr. David Alderton helped in the microthermometric analyses of the fluid inclusions at Royal Holloway and Bedford New College, University of London. We are also thankful to A. Zanchi and other reviewers for critically reviewing the manuscript and offering useful suggestions.

References

Absar A (1991) Hydrothermal epidote—an indicator of temperature and fluid composition. J Geol Soc India 38:625–628

Asrarullah (1982) Investigations for tungsten in Pakistan. In: Hepworth JV (eds) Tungst. Geol. Symp. Jiangxi. China, (ESCAP RMRDC). Bandung, Indonesia, pp 9–13

Benard F, Moutou P, Pichavant M (1985) Phase relations of tourmaline leucogranites and the significance of tourmaline in silicic magmas. J Geol 93:271–291

Beran A, God R, Gotzinger M, Zemann J (1985) A scheelite mineralization in calc-silicate rocks of the Moldanubicum (Bohemian Massif) in Austria. Mineral Deposits 20:16–22

Boissavy-Vinau M, Roger G (1980) The TiO_2/Ta ratio as an indicator of the degree of differentiation of tin granites. Mineral Deposits 15:231–236

Buchroithner MF (1980) An outline of the geology of the Afghan Pamirs. Tectonophysics 62:13–95

Christensen OD, Capuano RA, Moore JN (1983) Trace-element distribution in an active hydrothermal system, Roosevelt hot springs thermal area, Utah. J Volcanol Geotherm Res 16:99–129

Cullers RL, Yeh LT, Chaudhuri S, Guidotti CV (1974) Rare earth elements in Silurian pelitic schist from NW Maine. Geochim Cosmochim Acta 38: 389–400

Deer WA, Howie RA, Zussman J (1982) Rock-forming minerals, 1A, Orthosilicates, 2nd edn, London, pp 919

Deer WA, Howie RA, Zussman J (2013) An introduction to the rock-forming minerals. Min Soc Lond :498

Desio A (1966) The Devonian sequence in the Mastuj valley (Chitral, NW Pakistan). Riv Ital Paleontol Stratigr 72:293–320

Faisal S, Larson KP, King J, Cottle JM (2015) Rifting, subduction and collisional records from pluton petrogenesis and geochronology in the Hindu Kush NW Pakistan. Gondwana Res. doi:10.1016/j.gr.2015.05.014

Gaetani M, Leven E (1993) Permian stratigraphy and fusulinids from Rosh Gol (Chitral, E Hindu Kush). Riv Ital Paleontol Stratigr 99:307–326

Giere R (1990) Hydrothermal mobility of Ti, Zr and REE: examples from the Bergell and Adamello contact aureoles (Italy). T Nov. 2:60–67

Giuliani G, Li YD, Sheng TF (1988) Fluid inclusion study of Xihuashan tungsten deposit in the southern Jiangxi province, China. Mineral Deposits 23:24–33

Grauch RI (1989) Rare earth elements in metamorphic rocks. In: Lipin BR, McKay GA (eds) Geochemistry and mineralogy of rare earth element. Min Soc Am Rev Min, vol 21. pp 147–167

Heuberger S, Schaltegger U, Burg J-P, Villa IM, Frank M, Dawood H, Hussain, Zanchi A (2007) Age and isotopic constraints on magmatism

along the Karakoram-Kohistan suture zone, NW Pakistan: evidence for subduction and continued convergence after India-Asia collision. Swiss J Geosci 100:85–107. doi:10.1007/s00015-007-1203-7

Hildebrand PR, Noble SR, Searle MP, Waters DJ, Parrish RR (2001) Old origin for an active mountain range: geology and geochronology of the eastern Hindu Kush, Pakistan. Geol Soc Am Bull 113:625–639

Hildebrand PR, Searle MP, Shakirullah Zafarali K, van Heijst HJ (2000) Geological evolution of the Hindu Kush, NW Pakistan: active margin to continent-continent collision zone. In: Khan M et al (eds) Tectonics of the Nanga Parbat syntaxis and the western Himalaya: Geol Soc London, Spec Pub. vol 170, pp 277–293

Hilderband PR, Noble SR, Searle MP, Parrish RR, Shakirullah (1998) Tectonic significance of 24 Ma crustal melting in the eastern Hindu Kush, Palistan. Geology 26:871–874

Hosking KFG (1982) A general review of the occurrence of tungsten in the world. In: Hepworth JV, Zhang YH (eds) Tungst. Geol. Symp. Jiangxi. China, (ESCAP RMRDC). Bandung, Indonesia, pp 59–86

Keppler H, Wyllie PJ (1991) Partitioning of Cu, Sn, Mo, W, U and Th between melt and aqueous fluid in the systems haplogranite-H2O-HCl and haplogranite-H2O-HF. Contrib Mineral Petrol 109:139–150

Krauskopf KB (1967) Introduction to geochemistry. McGraw-Hill, p 721

Le Fort P, Debon F, Sonet J (1980) The "lesser Himalayan" cordierite granite belt, typology and age of the pluton of Mansehra, Pakistan. Geol Bull Univ Peshawar Spec Issue 13:51–61

Leake RC, Fletcher CJN, Haslam HW, Khan B, Shakirullah (1989) Origin and tectonic setting of stratabound tungsten mineralisation within the Hindu Kush of Pakistan. J Geol Soc Lond 146:1003–1016

Lindstrom RM, Anderson DL (1985) Analytical neutron-capture gamma-ray spectroscopy: status and prospects. In: Ramau, S. (eds), Capture Gamma-ray Spectroscopy and Related Topics. Am. Inst. Physics, New York, p 810

Linnen RL, Williams-Jones AE (1993) Mineralogical constraints on magmatic and hydrothermal Sn-W-Ta-Nb mineralization at the Nong Sua aplite-pegmatite, Thailand. Eur J Mineral 5:721–736

Linnen RL, Lichtervelde MV, Cerny P (2012) Granitic pegmatites as sources of strategic metals. Elements 8:275–280

Lottermoser BG (1989a) Rare-earth element study of exhalites within the Willyama Supergroup, Broken Hill Block, Australia. Mineral Deposits 24:92–99

Lottermoser BG (1989b) Rare-earth element behaviour associated with stratabound scheelite mineralisation (Broken Hill, Australia). Chem Geol 78:119–134

Lottermoser BG (1992) Rare earth elements and hydrothermal ore formation processes. Ore Geol Rev 7:25–41

Maucher A (1976) The stratabound cinnabar-stibnite-scheelite deposits (discussed with examples from the Mediterranean region). In: Wolf KH (Eds) Handbook of Plimer IR (1984). The role of fluorine in the submarine exhalative systems with special reference to Broken Hill, Australia. Mineral Deposits, vol 19. pp 19–25

Neinavaie H, Thalmann F, Ataii B, Beran A (1989) Wolframite- and scheelite-bearing carbonate rocks of the Nock mountains, Austria: a new type of tungsten mineralisation in the eastern Alps. Mineral Deposits 24:14–18

Niedermayr G, Schroll E (1983) The tungsten distribution in rocks of the Western Hohe Tauern. In: Schneider HJ (ed) Mineral deposits of the Alps and of the Alpine Epoch in Europe. Springer-Verlag, Berlin, pp. 240–248

Pascoe EH (1924) General report of the Geological Survey of India for the year 1923. India Geol Sur Rec 55: part 1

Plimer IR (1984) The role of fluorine in the submarine exhalative systems with special reference to Broken Hill, Australia. Mineral Deposits 19:19–25

Plimer IR (1986) Tourmalinites from the Golden Dyke Dome, Northern Australia. Mineral Deposits 21:263–270

Plimer IR (1987) The association of tourmalinite with stratiform scheelite deposits. Mineral Deposits 22:282–291

Pudsey CJ, Coward MP, Luff IW, Shackleton RM, Windley BF, Jan MQ (1985) Collision zone between the Kohistan arc and the Asian plate in NW Pakistan. Trans R Soc Edinb 76:463–479

Raith JG, Prochaska W (1995) Tungsten deposits in the Wolfram schist, Namaqualand, South Africa: strata-bound versus granite-related genetic concepts. Econ Geol 90:1934–1954

Robb LJ (2005) Introduction to ore-forming processes. Black Sci Ltd, pp 373

Rubin JN, Henry CD, Price JG (1993) The mobility of zirconium and other "immobile" elements during hydrothermal alteration. Chem Geol 110: 29–47

Siddiqui RH, Jan MQ, Khan MA (2012) Petrology of Late Cretaceous lave flows from a Ceno-Tethyan island arc: the Raskoh arc, Balochistan, Pakistan. Asian J Earth Sci 59:24–38

Siddiqui RH, Khan Z, Hussain SA (1986) Xenothermal alteration and tungsten mineralization in Saindak area, Baluchistan, Pakistan. Act Min Pak 2:74–77

Slack JF, Herriman N, Barnes RG, Plimer IR (1984) Stratiform tourmalinites in metamorphic terranes and their geologic significance. Geology 12: 713–716

Sonnet P, Verkaeren J, Crevola G (1985) Scheelite bearing calc-silicate gneisses in the Provence crystalline basement (Var, France). Bull Mineral 108:377–390

Spooner ETC (1981) Fluid inclusion studies of hydrothermal ore deposits. In: Hollister LS, Crawford ML (eds) Short course in fluid inclusion: App Pet 6, Min Ass Canada, pp 209–240

Stilling A, Cerny P, Vanstone PJ (2006) The Tanco pegmatite at Bernic Lake, Manitoba, XVI, zonal and bulk compositions and their petrogenetic significance. Can Mineral 44:599–623

Taylor SR (1965) The application of trace element data to problems in petrology. Phys Chem Earth 6:135–213

Taylor SR, McLennan SM (1985) The Continental crust: its composition and evolution. Black Sci Pub Oxford, p 312

Taylor RP, Ikingura JR, Fallick AE, Yiming H, Watkinson DH (1992) Stable isotope compositions of tourmalinites from granites and related hydrothermal rocks of the Karagwe-Ankolean belt, Northwest Tanzania. Chem Geol 94:215–227

Thalhammer OAR, Stumpfl EF, Jahoda R (1989) The Mittersill scheelite deposit, Austria. Econ Geol 51:1153–1171

Tukiainen T (1988) Niobium-tantalum mineralisation in the Motzfeldt Centre of the Igaliko nepheline syenite complex, South Greenland. In: Boissonnas J, Omenetto P (eds) Mineral deposits within the European Community. Springer-Verlag, Berlin, pp. 230–246

Turekian KK, Wedepohl KH (1961) Distribution of the elements in some major units of the earth crust. Geol Soc Am Bull 72:175–192

Van de Haar AJ, Vriend SP, van Gaans PFM (1993) Hydrothermal alteration of the Beira schist around the W-Sn specialised Regoufe granite, NW Portgal. J Geochem Explor 46:335–347

Wood SA (1990) The aqueous geochemistry of the rare earth elements and yttrium: 2. Theoretical predictions of speciation in hydrothermal solutions to 350 °C at saturation water vapor pressure. Chem Geol 88:99–125

Zahid M (1996) Genesis of stratabound scheelite and stratiform Pb-Zn mineralisation Chitral, Northern Pakistan, and its comparison with S-WEngland tin-tungsten deposits. Unpubl PhD thesis, University of Leicester, UK

Zahid M, Arif M, Moon CJ (2013) Petrogenetic implications of the mineral-chemical characteristics of scheelite and associated phases from Miniki Gol (Chitral), NW Pakistan. Geosci J 17(4):403–416

Zanchi A, Gaetani M (2011) The geology of the Karakoram range, Pakistan: the new 1:100,000 geological map of Central-Western Karakoram. Ital J Geosci (Boll So Geol It) 130(2). doi: 10.3301/IJG.2010.26

Zanchi A, Poli S, Fumagalli M, Gaetani M (2000) Mantle exhumation along the Tirich Mir fault zone, NW Pakistan: pre-mid-Cretaceous accretion of the Karakoram terrane to the Asian margin. In: Khan MA et al (eds) Tectonics of the Nanga Parbat syntaxis and the western Himalaya: Geol Soc London, Special Publication, vol 170, pp 277–293